

The influence of bedrock river morphology and alluvial cover on gravel entrainment. Part 2: Modelling critical shear stress

Rebecca A. Hodge¹  | Marcus E. H. Buechel² 

¹Department of Geography, Durham University, Durham, UK

²School of Geography and the Environment, University of Oxford, Oxford, UK

Correspondence

Rebecca A. Hodge, Department of Geography, Durham University, South Road, Durham, DH1 3LE, UK.

Email: rebecca.hodge@durham.ac.uk

Abstract

The critical shear stress (τ_c) at which grains are entrained on a bedrock surface is important for determining how bedrock rivers evolve through changes in sediment cover and bedrock erosion. The difference in τ_c for grains on bedrock and alluvial surfaces also determines whether a channel may be susceptible to runaway alluviation. Bedrock channel beds can have a wide variety of morphologies, but we do not fully understand how this variation affects τ_c . Here we address how bedrock morphology alters the grain entrainment parameters of pivoting angle, grain exposure and roughness height z_0 , and thus τ_c . In our companion article we used scaled, 3D printed replicas of seven bedrock surfaces to measure grain pivoting angles for four grain sizes. For three surfaces, pivoting angles were also measured with 25–100% sediment cover. In this second article, we combine these pivot angle data with measurements of grain exposure and surface roughness (standard deviation of elevations, σ_z) to predict τ_c using a force–balance model. The bedrock topography produces substantial variation in τ_c ; for a given grain diameter (D), a $3.6\times$ range of σ_z across the surfaces without sediment cover produces up to a $5.1\times$ variation in τ_c . For comparison, for any single surface, τ_c varies by up to $2.5\times$ for a fourfold range in grain size. Comparison to previous models with less representation of grain-scale geometry shows that in our results grains move at lower values of dimensionless critical shear stress (τ_c^*), and that τ_c^* decreases more quickly with increasing D/σ_z . However, direct comparison is difficult because previous relationships are based on a hydraulic roughness length that cannot be easily predicted without hydraulic data. Our results propose a new relationship between D/σ_z and τ_c^* , but further development and testing require datasets that combine measurements of flow, τ_c and grain-scale geometry.

KEYWORDS

bedrock river, critical shear stress, grain entrainment, pivot angle, surface roughness

1 | INTRODUCTION

Much literature has focused on the factors determining sediment entrainment and transportation in alluvial rivers, but there is far less understanding of their bedrock counterparts (Wohl, 2015). Understanding grain entrainment in bedrock rivers is critical for predicting both sediment transport rates and the development of sediment cover. Studies in alluvial rivers have demonstrated how the way in which sediment grains are arranged affects critical shear stress (τ_c); for example,

the impact of grain protrusion (Fenton & Abbott, 1977), grain geometry (Carling et al., 1992) and alluvial cover structure (Kirchner et al., 1990). The presence of exposed bedrock and thin alluvial cover in bedrock channels has been shown to cause sediment transport processes to be different from those in alluvial channels (Chatanantavet & Parker, 2008; Goode & Wohl, 2010; Hodge et al., 2011), but a complete understanding of these interactions is lacking.

Field and flume evidence from bedload tracers suggests that sediment entrainment from bedrock surfaces requires a lower τ_c than for

This is an open access article under the terms of the [Creative Commons Attribution](https://creativecommons.org/licenses/by/4.0/) License, which permits use, distribution and reproduction in any medium, provided the original work is properly cited.

© 2022 The Authors. *Earth Surface Processes and Landforms* published by John Wiley & Sons Ltd.

the same-size grains on alluvial surfaces (Ferguson et al., 2017; Hodge et al., 2011; Inoue et al., 2014). However, it has been suggested that for grains on rough bedrock surfaces τ_c could be higher than for alluvial surfaces (Johnson, 2014). There is also evidence that variations in τ_c with grain size may be smaller over bedrock surfaces than in alluvial channels, causing sediment transport to be less size selective than in adjacent alluvial reaches (Ferguson et al., 2017; Hodge et al., 2011). As well as affecting sediment transport rates, differences in τ_c on bedrock and alluvial surfaces also affects the development of sediment cover. If τ_c is higher for alluvial patches compared to the surrounding bedrock, then the initiation of sediment cover can cause runaway alluviation, whereby sediment grains encountering the sediment patch become less mobile and the area of sediment cover spreads rapidly (Chatanantavet & Parker, 2008; Demeter et al., 2005; Johnson, 2014).

We expect that at least some of the observed differences in τ_c between bedrock and alluvial reaches are because of the impact of the underlying bedrock surface on the grain-scale geometry (e.g., grain pivot angle and exposure), but these effects have not yet been quantified. More generally, the impact of bedrock topography on τ_c is often not considered when predicting bedload transport in bedrock channels. Previous attempts have often used a constant dimensionless critical shear stress (τ_c^*) and only incorporated the impact of varying bedrock and alluvial roughness on the flow (Bartels et al., 2021; Nelson & Seminara, 2012). Even when the impact of bedrock surfaces on τ_c^* is considered (e.g., Inoue et al., 2014; Johnson, 2014; Mishra & Inoue, 2020), the focus has still primarily been on the effect of bedrock surface roughness on flow via a hydraulic roughness length.

The aim of this pair of articles was to determine how the properties of bedrock surfaces with and without sediment cover affect the grain-scale geometry of sediment grains (i.e., pivot angle and exposure) and consequently τ_c . We address our aim using a novel set of 3D-printed replica bedrock surfaces. In the first article (Buechel et al., 2022), we reported how surface properties and grain pivot angles vary between surfaces, and with different percentages (0–100%) of alluvial cover; and we assessed relationships between these pivot angles and different methods of quantifying surface roughness.

In this article, we evaluate how variation in bedrock topography affects the entrainment parameters of pivot angle, roughness length and grain exposure. We then use Kirchner et al.'s (1990) grain entrainment model to assess how variation in the parameter values propagates through to variation in τ_c . From this, we assess how bedrock topography affects τ_c , and identify which parameters are most important to constrain for improved τ_c predictions. We then compare our results to entrainment models for bedrock rivers developed by Inoue et al. (2014) and Johnson (2014). By focusing on grain-scale geometry, we isolate the influence of the riverbed morphology on grain entrainment and remove the influence of other factors such as turbulent sweeps and instantaneous pressure gradients in the water column (Schmeeckle et al., 2007; Vollmer & Kleinhans, 2007) and channel slope (Lamb et al., 2008).

1.1 | Modelling grain entrainment from alluvial surfaces

To predict τ_c at the point of grain entrainment, we use the simple force-based model of Kirchner et al. (1990). At the point when the grain is about to mobilise, the following force balance occurs:

$$\frac{F_D}{\tan \phi} + F_L = F_W = \frac{1}{6}(\rho_s - \rho)g\pi D^3 \quad (1)$$

where F_L is the lift force, ϕ is the grain pivot angle, F_W is the grain weight, ρ_s is the density of sediment (taken as 2650 kg m⁻³), ρ is the density of water, g is acceleration due to gravity and D is the grain diameter. The model of Kirchner et al. (1990) calculates the shear stress that solves Equation 1.

F_D and F_L are calculated assuming a logarithmic relationship between flow velocity and height above the bed:

$$u(z) = \sqrt{\tau/\rho\kappa}^{-1} \ln\left(\frac{z+z_0}{z_0}\right) \quad (2)$$

where $u(z)$ is the flow velocity at height above the bed z , τ is the boundary shear stress, κ is von Kármán's constant (taken as 0.407) and z_0 is the roughness height. In Kirchner et al.'s (1990) original alluvial application, z_0 is 0.1 D_{B4} (Whiting & Dietrich, 1990). The reference height $z = 0$ is assumed to be the local mean bed elevation. Equation 2 is only applicable when $z > 0$; otherwise $u(z) = 0$. F_D is calculated as

$$F_D = \frac{C_D}{2} \rho \int_{p-e}^p w(z)u(z)^2 dz \quad (3)$$

where $w(z)$ is the width of the grain cross-section at height z ; C_D is an empirical drag coefficient assumed to be 0.4 (Wiberg & Smith, 1985); p and e are, respectively, grain protrusion and exposure, where protrusion is the height of the grain above the local mean bed elevation and exposure is the height of the grain above the local maximum upstream bed elevation; and F_L is calculated as

$$F_L = \frac{C_L}{2} \rho A [u(p)^2 - u(p-D)^2] \quad (4)$$

where A is the plan view cross-sectional area of the grain and C_L is an empirical lift coefficient assumed to be 0.2 (Wiberg & Smith, 1985). The boundary shear stress at the threshold of motion, τ_c , is calculated by rearranging the preceding equations and assuming that grains have a circular cross-section (for the full derivation, see Kirchner et al., 1990):

$$\tau_c = 0.1m(\rho_s - \rho)g\left(\frac{\pi D^3}{6}\right) \left\{ \frac{C_D}{\tan \phi 2\kappa^2} \int_{p-e}^p \sqrt{D^2 - [2z - (2p - D)]^2} f(z)^2 dz + \frac{\pi C_L}{8\kappa^2} D^2 [f(p)^2 - f(p-D)^2] \right\}^{-1} \quad (5)$$

where

$$f(z) = \ln\left(\frac{z+z_0}{z_0}\right) \quad z > 0 \\ f(z) = 0 \quad z \leq 0 \quad (6)$$

The original equation of Kirchner et al. (1990) is multiplied by 0.1 so that inputs in SI units produce a value of τ_c in Pa. We convert these values to τ_c^* using $\tau_c^* = \tau_c/(\rho_s - \rho)gD$. Although more recent entrainment models such as those of Vollmer and Kleinhans (2007) and Lamb

et al. (2008) have a more complete treatment of the hydraulics around the grain, our focus is on the impact of grain geometry on entrainment, and so, following the approach of Yager et al. (2018), the simpler Kirchner model is sufficient for this study.

1.2 | Modelling grain entrainment from bedrock surfaces

We compare our findings with Inoue et al.'s (2014) and Johnson's (2014) models for entrainment on bedrock surfaces. Both models incorporate differences between alluvial and bedrock surfaces through the effect of bedrock surface roughness. The main effect that is included in both is the effect of surface roughness on the near-bed hydraulics. Inoue et al. (2014) assumed that the grain would entrain through sliding on a smooth surface and did not incorporate the effects of bedrock roughness on pivot angle or grain exposure. At the point of motion:

$$F_D + F_W \sin \theta = (F_W \cos \theta - F_L) \mu_f \quad (7)$$

where θ is the bed slope angle and μ_f is the static friction coefficient. This is developed and rearranged to give the following equation for τ_c^* (see Inoue et al., 2014, for full derivation and justification of parameter values. Note also that the square is missing in eq. 16a in the original paper):

$$\tau_c^* = \alpha_1 / \left[\frac{1}{\kappa} \ln \frac{30.1 a_* D}{k_{sb}} \right]^2 \quad (8)$$

where

$$\alpha_1 = \frac{2A_3(\mu_f - \tan \theta) \cos \theta}{C_D A_2(\mu_f k_L + 1)} \quad (9)$$

in which a_* is a dimensionless coefficient relating the local flow velocity to the height above the bed, taken to be 0.65; k_{sb} is the hydraulic roughness height (note that this is different from z_0); A_3 is $\pi/6$ and A_2 is $\pi/4$; k_L is the ratio of lift forces to drag forces, taken to be 0.85; and μ_f is taken to be 0.75. Inoue et al. (2014) found that their model was able to reproduce values of τ_c^* measured in a flume experiment, using values of k_{sb} back-calculated from the hydraulic flume data.

Johnson (2014) indirectly incorporated grain geometry effects by developing the hiding function of Wilcock and Crowe (2003) for mixed-size alluvial beds. This function was originally designed to represent the increase or decrease in τ_c that is experienced by grains that are respectively smaller or larger than the median grain size (D_{50}). Johnson (2014) applied this model to bedrock rivers by scaling τ_c as a function of the grain size relative to a measure of the bedrock roughness:

$$\tau_c = \tau_{c_{ref}}^* (\rho_s - \rho) g r_{br} \sigma_z \left(\frac{D}{r_{br} \sigma_z} \right)^{b_r} \quad (10)$$

$$b_r = \frac{0.67}{1 + \exp \left(1.5 - \frac{D}{r_{br} \sigma_z} \right)} \quad (11)$$

where $\tau_{c_{ref}}^*$ is a reference dimensionless critical shear stress for grains on alluvium, assumed to be 0.055; and r_{br} is a fitting parameter

relating the standard deviation of surface elevations (σ_z) to a length scale equivalent to D_{50} in the alluvial scenario. We also use r_{br} to calculate z_0 when applying the Kirchner et al. (1990) model. Johnson (2014) used a range of flume data to determine possible parameter values for r_{br} but did not directly compare the predicted shear stresses to measured values.

2 | METHODS

2.1 | Summary of methods from companion paper

To produce the 3D printed surfaces used in these experiments, we used high-resolution topographic data of exposed bedrock channel beds, collected using terrestrial laser scanning of the River Garry (Scotland) and structure from motion (SfM) photogrammetry from North Wash (Utah, USA). Selected areas of these data were down-scaled and processed to produce a 3D printed tile, with maximum horizontal dimensions of 0.27×0.27 m. We started with four surfaces (S1, M1, M2 and R1, where S/M/R refer to smooth/medium/rough). R1 has a strong directionality to the topography, and so was analysed in two perpendicular orientations (R1_{rot} being the rotated version). To extend the range of roughness across the surfaces, we also increased the dimensions of R1 and M2 by 100% and printed a section of those to produce R1_{x2} and M2_{x2}, giving seven surfaces in total. To assess the impact of sediment cover on surface topography and grain entrainment, we added 25%, 50%, 75% and 100% sediment cover of two different grain sizes (11 and 32 mm) to surfaces S1, R1 and R1_{x2}, producing a further 24 surfaces with partial or full alluvial cover. The topography of the covered surfaces was measured using SfM photogrammetry (Figure 1; see Buechel et al., 2022 for details).

To measure pivot angles, each tile was attached to a tilt table. A grid of 81×30 mm cells was overlain on the surface, and the pivot angle of each cell was measured three times by dropping a grain into the cell and tilting the table until the grain moved by at least one grain diameter. The pivot angle is the angle of the table at which the grain moved. For the surfaces without sediment cover, the measurements were repeated using four grain sizes (8, 11, 16 and 32 mm). For surfaces with sediment cover, the pivoting grain was the same size as the sediment cover. Further details of these methods are provided in the companion article (Buechel et al., 2022).

We quantify the roughness of the different surfaces using the standard deviation of elevations, σ_z , which is used to calculate z_0 . In the companion article we assessed how pivot angles correlated with surface roughness at different scales. We found that mean pivot angles correlated most with roughness calculated at spatial scales equivalent to the grain size or smaller, and when the roughness was also measured in the pivot direction. However, we do not apply those alternative roughness metrics here for two reasons. First, we need to quantify roughness to predict the impact of channel topography on the flow, which is likely to be different to the impact of the topography on pivot angles. Second, using σ_z enables comparison with the work of Johnson (2014).

2.2 | Application of Kirchner, Inoue and Johnson models

We use the model of Kirchner et al. (1990) to calculate τ_c for grains within each 30 mm measurement cell across all surfaces. To do this

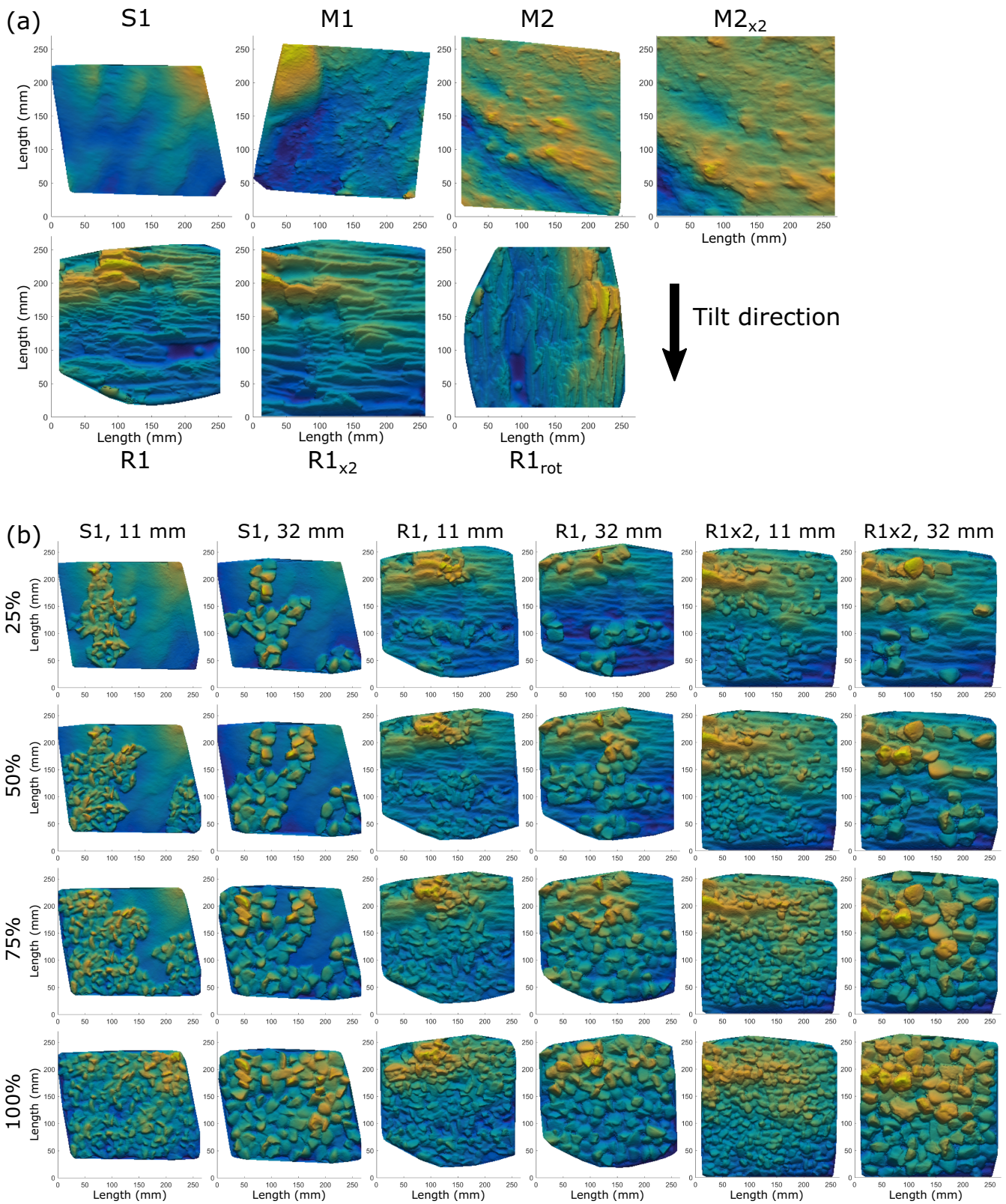


FIGURE 1 (a) Surfaces used in the experiments and (b) surfaces with varying amounts and sizes of sediment cover. Colour scale shows elevation and varies between surfaces to enhance visibility of the surface topography. Tilt direction indicates the downslope direction in the pivot angles experiments presented in the companion article (Buechel et al., 2022) [Color figure can be viewed at [wileyonlinelibrary.com](https://onlinelibrary.wiley.com)]

we require four parameters from our experiments: grain pivot angles, protrusion and exposure, and z_0 . We use the pivot angles from the experiments reported in Buechel et al. (2022). Grain protrusion is the maximum height of the grain above the mean bed elevation, indicating the vertical position of the grain within the velocity profile. We

assume that the base of each grain is at the mean bed elevation within each measurement cell, and so grain protrusion is therefore equal to the grain diameter. It is possible that grains sit within pockets that are lower than the mean bed elevation, and so our values of τ_c may be an underestimate. Setting the base of the grain at an elevation of one σ_z

below the mean elevation does, on average, double median τ_c for each surface. But it is unlikely that every measurement cell contains such a deep pocket. Identifying the minimum elevation at which different sized grains could sit in each cell requires detailed topographic analysis that is not consistent with the relatively simple approach taken elsewhere in this work. Furthermore, the sheltering effect of pockets in the bed is at least partially accounted for through our exposure measurements.

Grain exposure represents the sheltering effect of upstream obstacles and is the height difference between the top of the grain and the maximum upstream bed elevation. A zero or negative exposure means that the top of the grain is below the obstacle height, and therefore (in the Kirchner model) the grain will only be entrained by lift forces. For each measurement cell on the printed surfaces, we estimate exposure as the difference between the mean elevation of the measurement cell plus the grain diameter (i.e., the height of the top of the grain), and the 95th percentile of the elevations in the upstream (up-tilt) measurement cell. Pebble clusters have been found to influence flow over a downstream distance of up to 3.5 times the obstacle height (Lawless & Robert, 2001), and so an obstacle 8.6 mm high would affect the flow over the length of a measurement cell. For the roughest beds, over half the measurement cells have an upstream obstacle at least 8.6 mm high, suggesting exposure is being calculated over an appropriate downstream distance. For beds S1 and M2, no measurement cells have an upstream obstacle of that height. However, small obstacles only block the lowest velocity flows near the bed, and so overestimating the downstream influence of small obstacles is not problematic as such velocities do not greatly affect the calculated τ_c .

We use the 95th percentile of upstream elevations to calculate exposure rather than the maximum because a grain will be sheltered by a section of the topography rather than a single point, but our results are not sensitive to the exact percentile that is used. For example, using the 90th percentile decreases median τ_c for each surface by an average of 2% and a maximum of 7%, and using the 99th percentile increases median τ_c by an average of 4% and a maximum of 11%. In both cases, the pattern of median τ_c between different surfaces is not much altered. We calculate exposure when the bed is horizontal, and so our values are likely a minimum estimate as up-tilt sheltering could be higher when the bed is tilted.

To model the logarithmic flow profile, we need roughness length z_0 but there is no established method for calculating z_0 in bedrock channels. In alluvial channels, σ_z has been shown to be a better predictor of total flow resistance than D_{84} , but there is not necessarily a consistent scaling between the two (Aberle & Smart, 2003; Chen et al., 2020; Mishra & Inoue, 2020). Johnson (2014) estimated a bedrock hydraulic roughness length comparable to D_{84} as the product of σ_z and two scaling factors: r_{br} , which scales bedrock roughness to the D_{50} that would produce an equally rough alluvial surface; and r_d ,

which scales D_{50} to D_{84} . By comparing the measured hydraulic roughness and σ_z from flume experiments in bedrock channels and using r_{br} as a fitting parameter, Johnson (2014) determined that r_{br} varies from 1 to 5. Johnson set $r_d = 2$, representing D_{84} typically being about twice the size of D_{50} in an alluvial bed. We combine this approach with Kirchner et al.'s (1990) use of $z_0 = 0.1 D_{84}$, and so

$$z_0 = 0.1 r_d r_{br} \sigma_z \quad (12)$$

For most model runs, we use $r_{br} = 1$ and $r_d = 2$. We find that the resulting values of critical shear stress are sensitive to the value of r_{br} . Although we are primarily interested in the overall patterns, which are not dependent on this value, we also demonstrate this sensitivity by presenting a run using $r_{br} = 5$.

We ran the Kirchner model for each of the seven printed beds using three different parameterisations, as outlined in Table 1. Where z_0 is held constant, we use the same average value for all beds. For the beds without sediment cover, we calculate τ_c for the four grain sizes used in the pivot experiments. For beds with sediment cover, we calculate τ_c for grains the same size as the cover grains.

We compare our results to the Inoue et al. (2014) and Johnson (2014) models by using both to predict the relationship between τ_c^* and D/σ_z . To make predictions using Inoue et al.'s (2014) model, we need to identify values for k_{sb} , but do not have any hydraulic data. There is no established way to equate topographic properties to hydraulic roughness lengths, and the limited datasets suggest that there is not a one-to-one correlation between the two (e.g., Chatanantavet & Parker, 2008). Johnson (2014) specifies that the hydraulic roughness length for an alluvial bed is approximately equal to D_{84} , and therefore k_{sb} for a bedrock bed is approximately equal to $2r_{br}\sigma_z$. Inoue et al. (2014) predict τ_c^* as a function of D/k_{sb} —that is, $\frac{1}{2}D/r_{br}\sigma_z$ —and so to plot Inoue's predictions of τ_c^* as a function of D/σ_z we assume that r_{br} equals one, and rescale the x-axis accordingly. For the other parameters, we use the same values as specified in their original work. This includes the bed slope of 0.033, as a non-zero bed slope is needed for the model to run, and our printed surfaces do not have a net bed slope. However, we find that the model predictions are not sensitive to this value. To make predictions using Johnson's (2014) model, we use r_{br} values of one and five to define an envelope of τ_c^* values.

3 | RESULTS

3.1 | Entrainment parameter values

Before applying the model of Kirchner et al. (1990), we first consider the model parameters: pivot angle, z_0 , and grain exposure (Figure 2). For the beds without sediment cover, pivot angles (Figure 2b) are

TABLE 1 Combinations of parameterisations used in the Kirchner et al. (1990) model

Parameterisation	Pivot angle	z_0	Exposure
1	Experimental values	Constant (average σ_z from all beds)	Constant (no sheltering)
2	Experimental values	From σ_z for each bed	Constant (no sheltering)
3	Experimental values	From σ_z for each bed	Sheltering from upstream cell

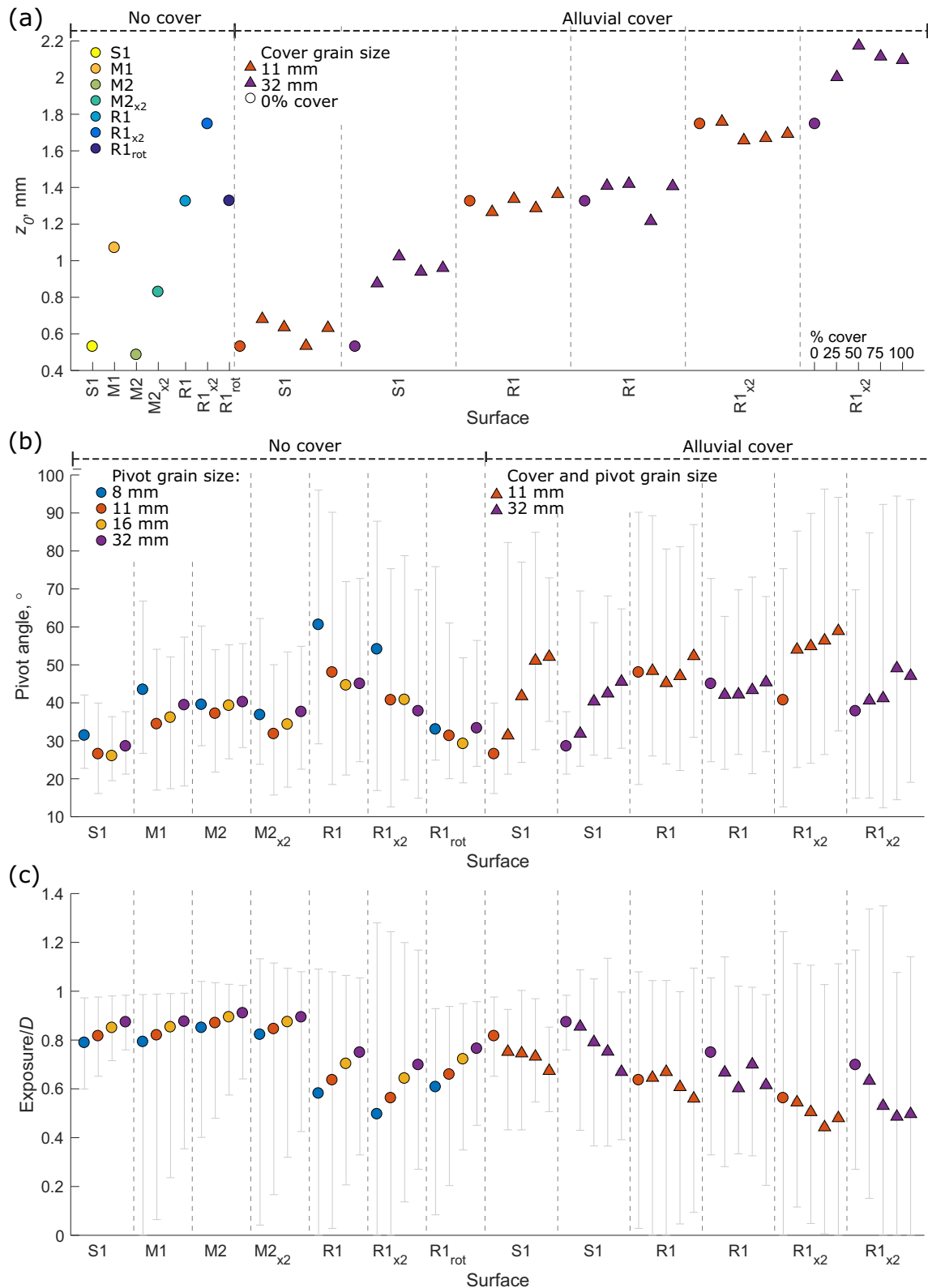


FIGURE 2 (a) Roughness height (z_0), (b) median pivot angles and (c) median grain exposure relative to grain size for all surfaces and amounts of sediment cover. Error bars in (b) and (c) show 5th and 95th percentiles [Color figure can be viewed at [wileyonlinelibrary.com](https://onlinelibrary.wiley.com)]

generally lower on the smoother surfaces (S1) and higher on the rougher surfaces (R1). The direction of surface structure is important, with pivot angles on R1_{rot} being far lower than on R1. There is little consistent pattern in how pivot angles vary with grain size; only for R1 and R1_{x2} does pivot angle decrease with increasing grain size. Adding sediment cover to surfaces S1 and R1_{x2} increases the

magnitude and range of pivot angles. However, for R1 sediment cover does not alter pivot angles. On all surfaces with sediment cover, 11 mm cover produces higher pivot angles than 32 mm cover, despite the cover and pivoting grains being the same size.

For the surfaces without sediment cover, z_0 is highest for surface R1_{x2}, and lowest for M2 (Figure 2a). For the surfaces with cover, z_0 is

similar to z_0 with 0% cover, with the exception of S1 and R1_{x2} with 32 mm cover, where the alluvial cover increases the value of z_0 . To compare grain exposure between different grain sizes, exposure is shown relative to grain size, so $e/D = 1$ is a fully exposed grain.) e/D increases with increasing grain size, and is roughly inverse to z_0 (Figure 2c). One exception to these patterns is that e/D is similarly high on S1, M1, M2 and M2_{x2}, despite M1 and M2_{x2} having higher z_0 values. Another exception is that, for most surfaces with alluvial cover, e/D decreases with increasing cover, whereas z_0 remains approximately constant.

3.2 | Application of the Kirchner et al. (1990) entrainment model

The first model parameterisation incorporated only our measured variation in pivot angles (Figure 3a). z_0 was held constant between surfaces (at the overall mean value of 1.3 mm) and we assumed zero upstream sheltering (i.e., protrusion and exposure are both equal to grain diameter). Despite a 2.3 times variation in median pivot angles across surfaces, the median value of τ_c across all surfaces only varies by 1.8 times, from 1.3 to 2.4 Pa. There is little systematic variation in median τ_c by grain size. In alluvial channels, τ_c^* is typically expected to be around 0.045 (Buffington & Montgomery, 1997; Miller et al., 1977). In comparison, for our data all 95th percentiles of τ_c are less than τ_c for an 8 mm grain when τ_c^* equals 0.045. Low percentiles

of τ_c represent when grains of that size start to be entrained, and so these percentiles could show that bedrock topography has differing impacts on the start and bulk of sediment transport. However, the 5th percentiles and medians of τ_c show a similar pattern.

The second and third model parameterisations also include the influence of the surface topography on the flow, and thus on τ_c (Figure 3b,c). The second parameterisation incorporates variation in z_0 between surfaces, and the third adds variation in upstream sheltering through grain exposure. In the second parameterisation, including the 4.5 times variation in z_0 between surfaces into the model increases the variation in τ_c , with median τ_c varying by 5.9 times (Figure 3b). Median τ_c and the range of τ_c decrease for surfaces where z_0 is smaller than the average value used in the first parameterisation (M1, M2_{x2}, S1 with and without sediment cover). Surfaces with higher than average z_0 (R1_{x2} with and without sediment cover) see an increase in the median and range of τ_c .

There is a twofold variation in median grain exposure across the different surfaces (Figure 2c). Incorporating this in the third parameterisation further increases the variability in τ_c between the surfaces to seven times, because median τ_c increases for surfaces with smaller exposure values (primarily R1 and R1_{x2} with and without sediment cover; Figure 3c). Under this model parameterisation and across the surfaces without sediment cover, grains of the same size have a variation of up to five times in median τ_c (Figure 3c), showing that surface topography can have an appreciable effect on sediment mobility. Development of sediment cover on these surfaces can cause median

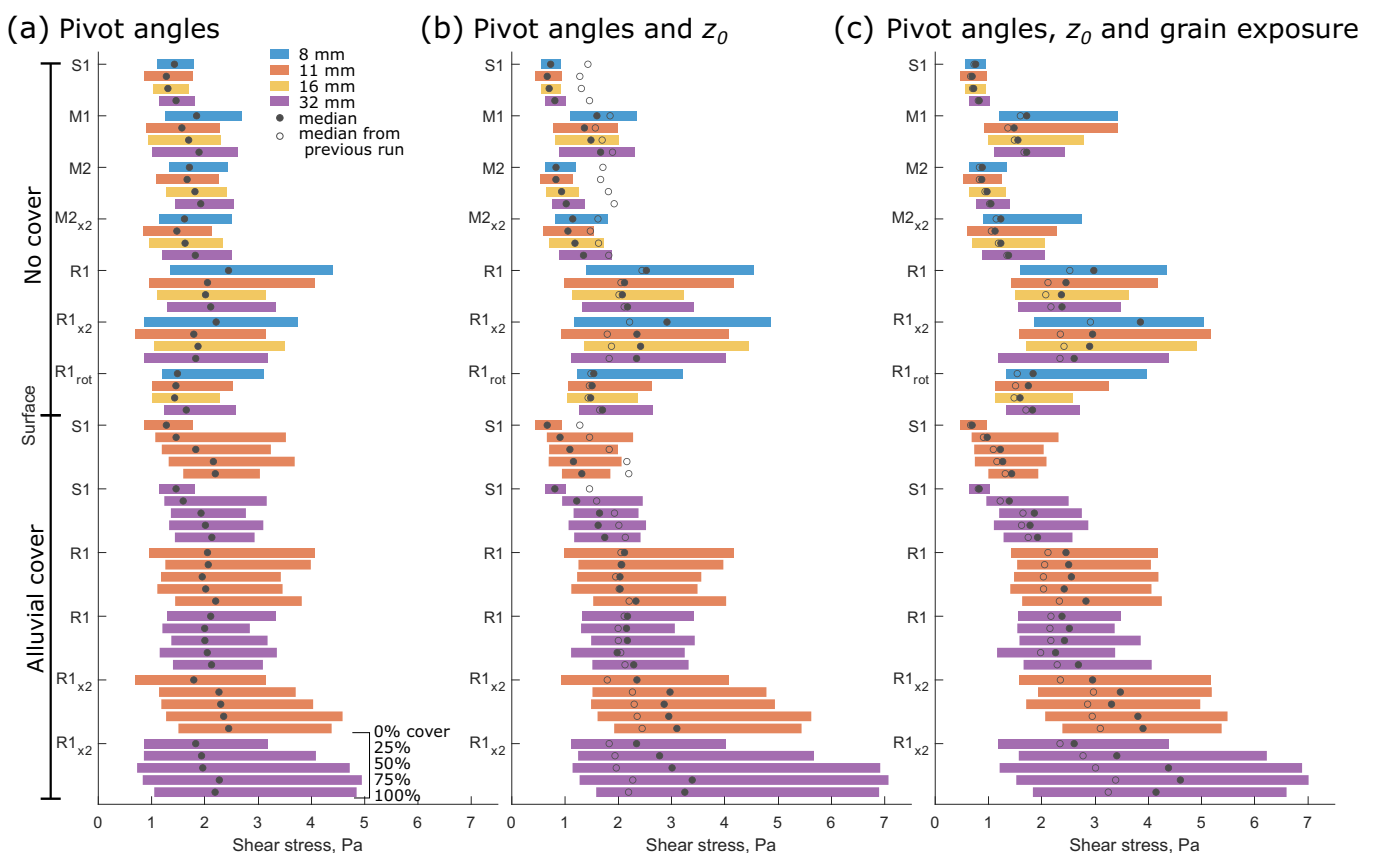


FIGURE 3 Distributions of critical shear stress (τ_c) for different surfaces and different alluvial cover extents, using the three different Kirchner model parameterisations: (a) Includes variation in pivot angles; (b) adds variation in z_0 ; and (c) adds variation in grain exposure. In (b) and (c) the median values from the previous parameterisation are shown for comparison. For context, the critical shear stress for an 8 mm grain at a dimensionless critical shear stress of 0.045 is 8.7 Pa [Color figure can be viewed at [wileyonlinelibrary.com](https://onlinelibrary.wiley.com/doi/10.1002/esp.5462)]

τ_c to double (Figure 3c). Patterns of the 5th percentile of τ_c are again similar to those for the median. For some surfaces where incorporating grain exposure does not change the median, the 95th percentile of τ_c still increases (e.g., M1, M2_{x2}).

Variations in surface topography have a larger impact on τ_c than variations in grain size. For uncovered surfaces, median τ_c is approximately constant across the different grain sizes, except for R1 and R1_{x2}, where it decreases (Figure 3c). On these two surfaces, the difference in τ_c between grain sizes increases between the first and third model parameterisations. For surfaces with sediment cover, increasing cover increases τ_c for both grain sizes on S1 and R1_{x2}, though not for R1. Even at 100% sediment cover, the underlying topography still affects τ_c ; different surfaces covered with the same grain size produce different τ_c , and R1_{x2} continues to have the highest τ_c .

Figure 4 shows that all three parameters (pivot angles, z_0 and exposure) contribute to τ_c^* in the final model. For surfaces with lower values of z_0 , z_0 explains most of the variation in median τ_c^* ; however, for surfaces with higher z_0 , the impact of exposure and pivot angles becomes more important (with overall $R^2 = 0.67$). Pivoting angle correlates less well with median τ_c^* ($R^2 = 0.63$), and grain exposure shows the strongest correlation ($R^2 = 0.79$). Generally, surfaces with higher roughness (z_0) values also have increased range of τ_c^* (Figure 4c), which reflects the increased variability in pivot angles and grain exposure values across these surfaces (Figure 2b,c).

3.3 | Comparison to the Inoue et al. (2014) and Johnson (2014) entrainment models

Plotting τ_c^* from the third model against D/σ_z does collapse the data from all surfaces (with and without sediment cover) into a single trend (Figure 5), more so than plotting against any single parameter (Figure 4). This suggests that some parameters compensate for each other. For example, grains on M1 and R1_{rot} have similar τ_c^* values. On surface R1_{rot}, grains are less exposed and z_0 is higher, reducing the flow velocity at a given height, but this is counteracted by lower pivot angles compared to M1.

Comparing our modelled values of τ_c^* to the values predicted by Inoue et al.'s (2014) and Johnson's (2014) models, we find Inoue et al.'s (2014) model produces a relationship between D/σ_z and τ_c^* that has a similar shape to our model results, but with values that are about 0.015 higher (Figure 5a). The two different parameterisations of Johnson's model (using r_{br} values of one and five) both produce predictions of τ_c^* that are much higher than our modelled values, despite our model and one of the predictions both using $r_{br} = 1$ to calculate z_0 . The Johnson (2014) model predicts that when D/σ_z is equal to one (and r_{br} is 1), then τ_c^* is equal to τ_{c-ref}^* , which Johnson (2014) sets at 0.055. In contrast, our bed/grain size combination with the smallest value of D/σ_z (1.4) has a median τ_c^* of 0.02. Finally, the Johnson (2014) model predicts that τ_c^*

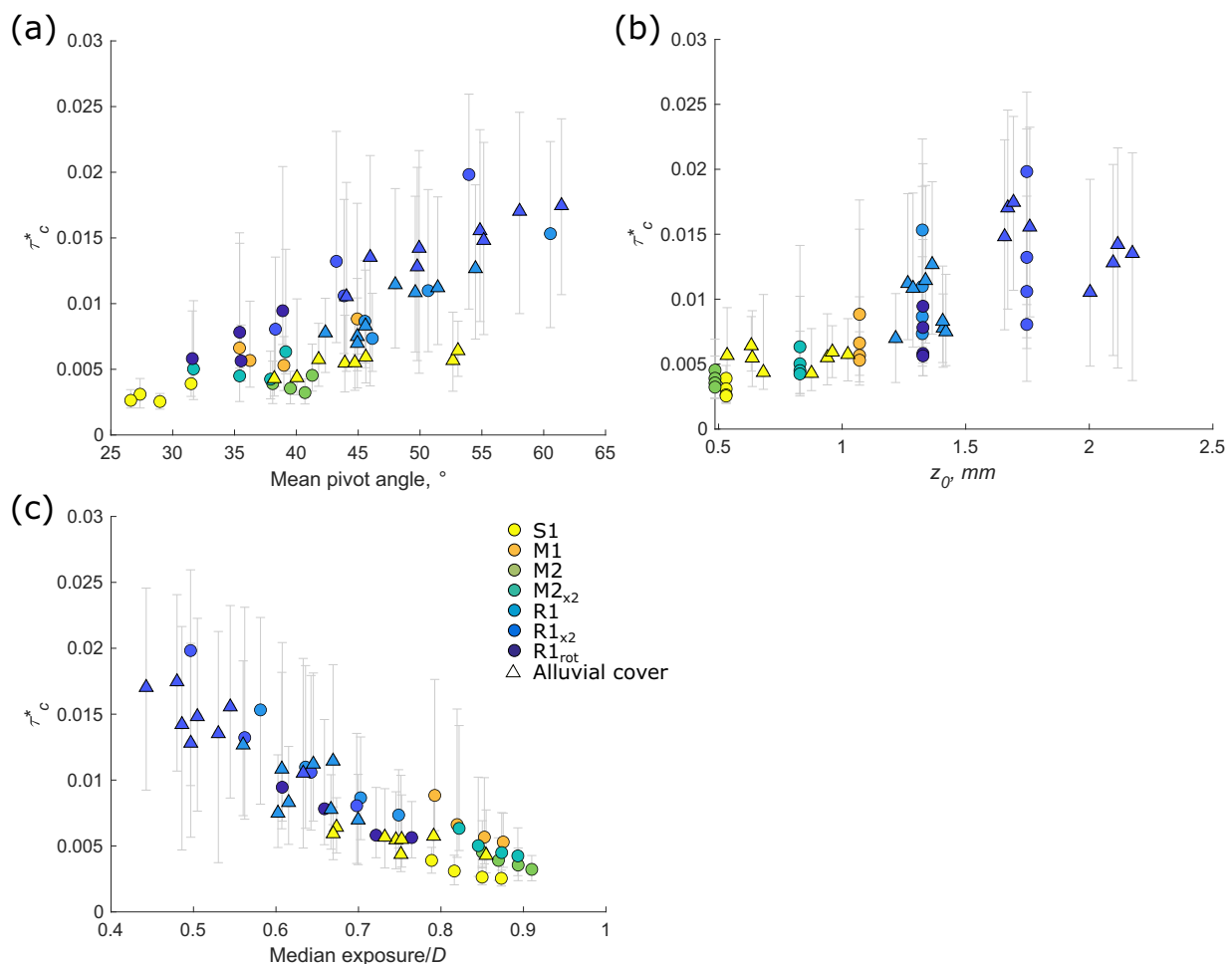


FIGURE 4 Relationships between median dimensionless critical shear stress (τ_c^*) and key model variables: (a) mean pivot angle; (b) roughness height z_0 ; and (c) exposure height relative to grain size. Error bars show 5th and 95th percentiles. R^2 for linear fits to the data are 0.63, 0.67 and 0.79, respectively [Color figure can be viewed at [wileyonlinelibrary.com](https://onlinelibrary.wiley.com)]

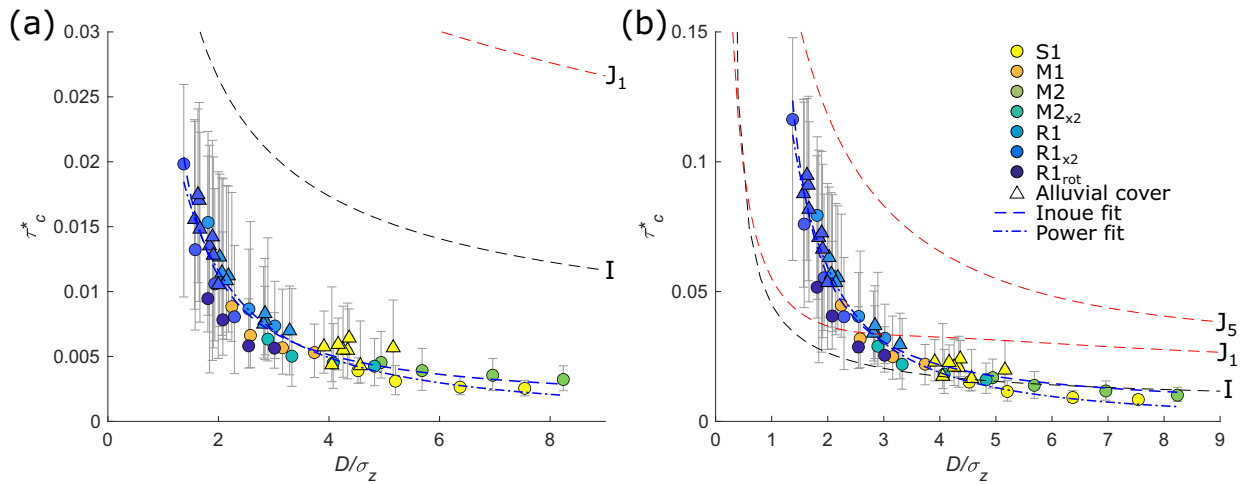


FIGURE 5 (a) Relationship between median dimensionless critical shear stress (τ_c^*) and D/σ_z using the final Kirchner model parameterisations (Table 1). (b) The same model parameterisation, but with a different multiplier used to calculate z_0 . Error bars show the 5th and 95th percentiles. Black and red lines are entrainment relationships from Inoue et al. (2014) and Johnson (2014), respectively. Johnson relationships use r_{br} values of one (J1) and five (J5). Point shapes distinguish runs with (triangles) and without (circles) sediment cover. Blue lines are relationships fitted to the data, which are either power functions or follow the form of Inoue's (2014) model. For (a) the relationships are $\tau_c^* = 0.15/(2.5 \ln[2.14 D/\sigma_z])^2$; $\tau_c^* = 0.03 (D/\sigma_z)^{-1.24}$; and for (b) the relationships are $\tau_c^* = 0.46/(2.5 \ln[1.58 D/\sigma_z])^2$, $\tau_c^* = 0.19 (D/\sigma_z)^{-1.66}$ [Color figure can be viewed at wileyonlinelibrary.com]

decreases more slowly with increasing D/σ_z than is shown by our modelled values.

We then explore the impact of the scaling factor, r_{br} , used to convert σ_z to z_0 . z_0 affects τ_c^* because it controls the rate at which flow velocity increases with elevation above the mean bed elevation. Following Johnson (2014), we used a value of 1 to calculate z_0 for our Kirchner et al. (1990) model calculations. Figure 5b shows a new run of the third parameterisation of the Kirchner et al. (1990) model using $r_{br} = 5$ instead. This increases our modelled values of τ_c^* into the range of values predicted by the Johnson (2014) model and shows that predictions of τ_c^* are sensitive to the value of z_0 . However, the shape of our τ_c^* values still does not match the shape of either of the Johnson curves.

To produce a predictive relationship, we fit two curves to our data. The first follows the form of Inoue's model (Equation 8), with the relationship

$$\tau_c^* = a / \left[\frac{1}{K} \ln \frac{bD}{K_{sb}} \right]^2 \quad (13)$$

where a and b are fitting parameters. For our data when $r_{br} = 1$ (Figure 5a), then $a = 0.148$ and $b = 2.137$. For the data when $r_{br} = 5$ (Figure 5b), then $a = 0.462$ and $b = 1.577$. a and b are respectively equivalent to α_1 and $30.1a$ in Equation 8. Using Equation 9 and the coefficient values identified by Inoue et al. (2014) gives α_1 equal to 1.5, and $30.1a$ equal to 19.6, which are higher than the values of a and b fitted to our data. α_1 decreases to 0.48 (close to our fitted b values) if the static friction coefficient (μ_f) is reduced from 0.75 to 0.2, which is below the lowest static friction coefficient of 0.3 reported by Byerlee (1978). Reducing $30.1a$ to our fitted b value of about 2 necessitates reducing the dimensionless height α^* from 0.65 to 0.066, which is not consistent with the flow assumptions made by Inoue et al. (2014). Consequently, fitting Equation 8 to our data may require coefficient values that are outside the range of likely values. The second curves we fit are power

laws, which have exponents of -1.24 when $r_{br} = 1$, and -1.66 when $r_{br} = 5$ (Figure 5).

4 | DISCUSSION

4.1 | The impact of bedrock topography on critical shear stress

The underlying bedrock topography can have a substantial impact on τ_c , even under 100% alluvial cover (Figure 3). Our results show that, across a range of D/σ_z from 1.4 to 8.2, the variation in τ_c for the same grain size between surfaces is greater than the difference in τ_c for different grain sizes on the same surface (Figure 3c). Of the three parameters, z_0 and grain exposure produce the most difference in τ_c between the different surfaces. The importance of z_0 provides support for previous approaches that only considered the impact of roughness on flow rather than grain geometry (e.g., Inoue et al., 2014). The combined impact of the surface topography on the entrainment parameters creates a power relationship between τ_c^* and D/σ_z with an exponent of -1.24 (when $r_{br} = 1$), such that increasing the size of the sediment grain relative to the surface roughness produces a disproportionate decrease in τ_c^* . For comparison, in the context of alluvial channels, a power relationship between τ_c^* and D/D_{50} with an exponent of -1 would indicate equal mobility. That is to say, any increase in grain size is balanced by an increase in grain exposure and decrease in pivot angle, such that all grain sizes move at the same τ_c (Andrews, 1983; Parker et al., 1982).

Decreases in τ_c^* with increasing D/σ_z may be disproportionately larger in the bedrock setting because of how the bedrock surface affects the entrainment parameters. Grains on a bedrock surface have a greater protrusion (height above mean bed elevation) compared to grains in an alluvial bed which are often at least 50% buried (Hodge et al., 2020; Yager et al., 2018). Consequently, bedrock grains will be more affected by changes in the flow profile and upstream sheltering.

As D/σ_z increases, there is a strong increase in z_0 and a strong decrease in median e/D , with a less clear trend for pivot angles (Figure 6). Decreasing z_0 and increasing relative exposure both increase grain mobility. The former changes the velocity profile, bringing higher velocity flows closer to the bed. The latter means that more of the grain's surface area is affected by the flow and so the grain is more sensitive to changes in σ_z and hence z_0 . The combined effect of these terms outweighs increases in grain resistance caused by increased grain weight. Such changes may be more rapid compared to the alluvial relationship between τ_c^* and D/D_{50} because in an alluvial bed there is no systematic trend between exposed area and D/D_{50} , and protrusion potentially decreases with increasing grain size (Hodge et al., 2020). Consequently, changes in exposure with D/D_{50} do not necessarily compensate for changes in grain weight.

Our modelled τ_c^* values are lower than those predicted by the models of Inoue et al. (2014) and Johnson (2014). However, comparison between our results and Inoue's model is complicated by the model's use of a hydraulic roughness length (k_{sb}) that we cannot measure directly. Inoue's (2014) model assumes that grains are entrained by sliding rather than pivoting, but our data do agree with the shape of the relationship produced by that model. However, fitting that relationship to our data requires some unlikely parameter values. Johnson's (2014) model plots above our data, partly because of his

assumption that τ_c^* is 0.055 when D/σ_z is one. However, on setting the reference τ_c^* to 0.02 in line with our modelled data, most of the curve still does not correspond to our data, as the model's rate of decrease in τ_c^* with increasing D/σ_z is not as rapid as in our data (Figure 5). This slower decrease may be because Johnson's (2014) model is based on Wilcock and Crowe's (2003) equations for hiding behaviour in alluvial beds, in which τ_c^* may not decrease as rapidly for the reasons outlined above.

4.2 | Comparison to bedload tracer measurements

For each exposed surface, our predictions of τ_c (Figure 3c) show equal mobility of the four grain sizes, with all sizes moving at low τ_c . The only exception is R1 and R1_{x2}, where τ_c is weakly inverse to grain size. This equal mobility and low τ_c are consistent with bedload tracer data from channels with high bedrock exposure (Ferguson et al., 2017; Hodge et al., 2011), where tracers on bedrock are mobilised at lower shear stresses than are tracers in alluvial patches, and where comparable travel distances for all grain sizes indicate that all sizes are mobilised at a similar shear stress. The bedrock bed in channels studied by Hodge et al. (2011) and Ferguson et al. (2017) did not have a strong directional structure, similar to our smooth and medium

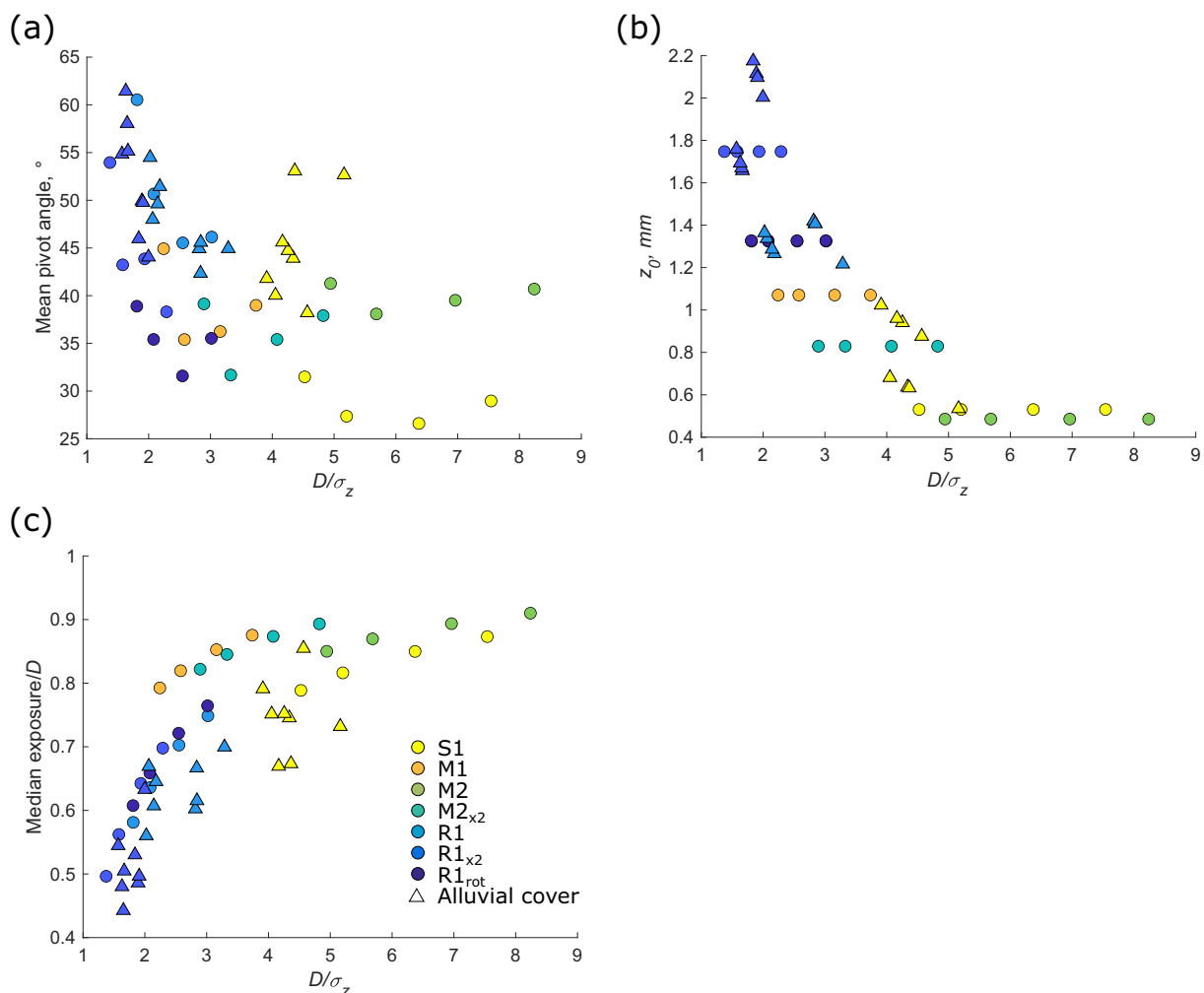


FIGURE 6 Relationships between grain size relative to the standard deviation of surface elevations (D/σ_z) and key model variables: (a) mean pivot angle; (b) roughness height z_0 ; and (c) exposure height relative to grain size [Color figure can be viewed at [wileyonlinelibrary.com](https://onlinelibrary.wiley.com)]

surfaces. A better comparison to R1 is provided by Goode and Wohl's (2010) bedload tracer data from the Ocoee River, which has bedrock ribs. They found that tracer travel distance was further and grain size dependent when the ribs were parallel to flow, and shorter and size independent when ribs were oblique to flow. The difference in travel distances is consistent with our finding that τ_c is lower when ribs are parallel ($R1_{rot}$), rather than perpendicular (R1), to the flow direction. But our data show the opposite pattern in grain size dependence, with less variation in τ_c between grain sizes with flow parallel ($R1_{rot}$), compared to flow perpendicular (R1), ribs. The difference could be because in the Ocoee River there was a greater spacing between the ribs relative to the grain size, which was filled with substantial sediment cover. Consequently, when the ribs were flow parallel, sediment entrainment may have been more similar to size-selective entrainment in alluvial channels (Church & Hassan, 1992; Ferguson et al., 1996; Haschenburger, 2013). Goode and Wohl (2010) also found that transport distances were best explained by local-scale bedrock topography and sediment architecture, consistent with our findings in the companion paper that pivot angles are best explained by small-scale roughness.

4.3 | Implications for sediment cover development

How τ_c changes with increasing cover has implications for predicting the relationship between sediment flux and sediment cover, which is important for modelling channel incision and landscape evolution (Lague, 2010; Sklar & Dietrich, 2004; Turowski, 2021). If sediment cover increases τ_c , in turn making sediment grains less mobile, then this positive feedback can produce rapid deposition of sediment cover, known as runaway alluviation (Chatanantavet & Parker, 2008; Demeter et al., 2005; Finnegan et al., 2007). Surfaces S1 and $R1_{x2}$ show potential for runaway alluviation, as τ_c increases with increasing cover (Figure 3c). In contrast, the surface with intermediate roughness (R1) does not, as τ_c does not change with increasing cover. These patterns of changes in τ_c with increasing cover are the same as those for pivot angles, showing the importance of small-scale bed roughness for predicting sediment dynamics.

Inoue et al. (2014) distinguished between clast-smooth and clast-rough surfaces by comparing the roughness of the underlying bedrock and overlying sediment cover. Sediment cover development on clast-smooth surfaces theoretically increases overall roughness and τ_c , increasing the likelihood of further sediment deposition, producing runaway alluviation. By Inoue et al.'s (2014) definition, our surfaces are all clast-smooth (see companion article), but R1 does not show the potential for runaway alluviation. Furthermore, the two surfaces that do, S1 and $R1_{x2}$, are respectively smoother and rougher than R1, and so the difference in behaviour cannot be explained only through overall roughness σ_z . The clast-smooth/clast-rough distinction may therefore be a useful starting point, but does not fully represent the sediment dynamics.

One caveat to consider is that we have focused on the entrainment of individual grains from bedrock and alluvial surfaces (following the approach of Kirchner et al., 1990). When there is partial or full alluvial cover, we have focused on grains that are placed on top of, or adjacent to, the sediment patches. Such locations are where new grains will be deposited, and where erosion of the sediment cover

tends to initiate (Hodge & Hoey, 2016). However, as sediment patches expand, newly deposited grains can become surrounded by other grains, decreasing exposure, and increasing pivot angles and thus τ_c . Entrainment of such grains will also be inhibited by the weight of overlying grains (Sanguinito & Johnson, 2012; Yager et al., 2018) and the development of any grain-scale structures (Hassan et al., 2020; Lamarre & Roy, 2008), both of which are not considered in our analysis. Consequently, our reported τ_c is not representative of grains in the middle of the patches. It is therefore possible that, for R1, run-away alluviation may still occur because of grains becoming incorporated into patches, even if newly deposited grains are equally likely to be entrained from bedrock or alluvial areas.

The idea of τ_c changing as sediment is deposited or eroded on a bedrock surface is similar to that developed by Johnson (2016) for alluvial channels, in which τ_c changes as a state function of sediment supply and thus erosion or deposition. In the alluvial example, erosion increases τ_c as grains in more mobile positions are preferentially entrained (as also observed by Mao, 2012; Masteller & Finnegan, 2017; Ockelford & Haynes, 2012), and τ_c decreases with deposition as grains are deposited in increasingly less stable locations, providing a negative feedback on bed stability. This approach could be extended for bedrock rivers, predicting variation in τ_c both with erosion/deposition and the extent of bedrock exposure. However, our results show that bedrock topography still influences τ_c even at 100% sediment cover, and so such an approach may also need to consider sediment depth or some other metric that determines the point at which underlying bedrock topography stops influencing sediment transport dynamics.

Inoue et al.'s (2014) and Johnson's (2014) models of τ_c are a useful starting point for developing a state function, although the model results are sensitive to parameters such as r_{br} that need to be better constrained (Figure 5). Encouragingly, Mishra and Inoue's (2020) attempt to fit r_{br} using a new flume dataset produced similar values to those identified by Johnson (2014). New methods such as the transform-roughness correlation to predict roughness lengths directly from channel topography (Adams & Zampiron, 2020) would also facilitate the application of these models. Predicting τ_c as a function of erosion/deposition and bedrock exposure would be useful for applications including landscape evolution modelling. However, the finding that τ_c is most dependent on z_0 and grain exposure, and consequently bed topography at the grain scale is potentially problematic as landscape evolution models cannot reproduce channel properties at this level of detail. To implement such a model, further understanding is needed of whether small-scale channel topography can be predicted from larger-scale factors such as lithology, sediment supply, discharge, channel slope and width.

5 | CONCLUSIONS

Bedrock surfaces affect τ_c of overlying grains by altering pivot angles, grain exposure and local flow conditions in ways that are still difficult to predict. Here we have reported how these parameters vary for grains on a range of bedrock topographies with and without different extents of sediment cover, and we have used the Kirchner et al. (1990) model to predict τ_c for these grains. Across a range of D/σ_z from 1.4 to 8.2, we find that variations in topography between the

surfaces have a larger impact on τ_c than variations in grain size, and that values of τ_c are primarily controlled by the impact of topography on z_0 and grain exposure. Our values of τ_c^* are similar to the model of Inoue et al. (2014), though direct comparison is difficult because their model is based on a hydraulic roughness length that cannot robustly be calculated from topographic data. Comparison to Johnson's (2014) model suggests that, as D/σ_z increases, τ_c^* decreases faster than in the comparable scenario of hiding effects in a mixed alluvial bed. Our results provide a relationship to predict τ_c^* as a function of D/σ_z , though this relationship still must be comprehensively tested. Overall, our results show grain-scale geometry can produce substantial variations in τ_c^* . However, new datasets that combine measurements of flow, τ_c^* and grain geometry would enable our approaches to be more robustly compared to alternative methods, and hence develop better predictive equations.

ACKNOWLEDGEMENTS

We thank Mervyn Brown for helping set up the experiment and Dr Kamal Badreshany (Durham Archaeomaterials Research Centre) for printing the 3D bedrock surfaces. We also acknowledge Dr Richard Williams and Eleanor Reid for collecting the River Garry terrestrial laser scanner data, and Dr Joel Johnson, Prof. Elwyn Yager and Dr Andy Tranmer for their assistance in collecting the North Wash data.

CONFLICT OF INTEREST

We declare no financial interests.

AUTHOR CONTRIBUTIONS

RAH and MEHB jointly designed the study. RAH undertook the analysis and modelling, and wrote the paper. MEHB edited the paper.

DATA AVAILABILITY STATEMENT

The model output datasets are available on zenodo: <https://doi.org/10.5281/zenodo.6798180>.

ORCID

Rebecca A. Hodge  <https://orcid.org/0000-0002-8792-8949>

Marcus E. H. Buechel  <https://orcid.org/0000-0002-5047-1631>

REFERENCES

- Aberle, J. & Smart, G.M. (2003) The influence of roughness structure on flow resistance on steep slopes. *Journal of Hydraulic Research*, 41(3), 259–269. Available from: <https://doi.org/10.1080/00221680309499971>
- Adams, D.L. & Zampiron, A. (2020) Short communication: Multiscalar roughness length decomposition in fluvial systems using a transform-roughness correlation (TRC) approach. *Earth Surface Dynamics*, 8(4), 1039–1051. Available from: <https://doi.org/10.5194/esurf-8-1039-2020>
- Andrews, E.D. (1983) Entrainment of gravel from naturally sorted riverbed material. *Geological Society of America Bulletin*, 94(10), 1225–1231. Available from: [https://doi.org/10.1130/0016-7606\(1983\)94<1225:EOGFS>2.0.CO;2](https://doi.org/10.1130/0016-7606(1983)94<1225:EOGFS>2.0.CO;2)
- Bartels, G.K., dos Castro, N.M.R., Collares, G.L. & Fan, F.M. (2021) Performance of bedload transport equations in a mixed bedrock–alluvial channel environment. *Catena*, 199, 105108. Available from: <https://doi.org/10.1016/j.catena.2020.105108>
- Buechel, M.E.H., Hodge, R.A. & Kenmare, S. (2022) The influence of bedrock river morphology and alluvial cover on gravel entrainment: Part 1. Pivot angles and surface roughness. *Earth Surface Processes and Landforms*.
- Buffington, J.M. & Montgomery, D.R. (1997) A systematic analysis of eight decades of incipient motion studies, with special reference to gravel-bedded rivers. *Water Resources Research*, 33(8), 1993–2029. Available from: <https://doi.org/10.1029/96WR03190>
- Byerlee, J. (1978) Friction of rocks. *Pure and Applied Geophysics PAGEOPH*, 116(4–5), 615–626. Available from: <https://doi.org/10.1007/BF00876528>
- Carling, P., Kelsey, A. & Glaister, M. (1992) Effect of bed roughness, particle shape and orientation on initial motion criteria. In: Thorne, C.R., Bathurst, J.C. & Hey, R. (Eds.) *Sediment transport in gravel-bed rivers*. Chichester, UK: Wiley, pp. 23–37.
- Chatanantavet, P. & Parker, G. (2008) Experimental study of bedrock channel alluviation under varied sediment supply and hydraulic conditions. *Water Resources Research*, 44(12), 1–19. Available from: <https://doi.org/10.1029/2007WR006581>
- Chen, X., Hassan, M.A., An, C. & Fu, X. (2020) Rough correlations: Meta-analysis of roughness measures in gravel bed Rivers. *Water Resources Research*, 56(8), e2020WR027079. Available from: <https://doi.org/10.1029/2020WR027079>
- Church, M. & Hassan, M.A. (1992) Size and distance of travel of unconstrained clasts on a streambed. *Water Resources Research*, 28(1), 299–303. Available from: <https://doi.org/10.1029/91WR02523>
- Demeter, G.I., Sklar, L.S. & Davis, J.R. (2005) The influence of variable sediment supply and bed roughness on the spatial distribution of incision in a laboratory bedrock channel. *Eos Transactions AGU Fall Meeting Abstracts*, vol. 2005, pp. H53D-0519.
- Fenton, J.D. & Abbott, J.E. (1977) Initial movement of grains on a stream bed - effect of relative protrusion. *Proceedings of the Royal Society of London Series A-Mathematical*, 352(1671), 523–537. Available from: <https://doi.org/10.1098/rspa.1977.0014>
- Ferguson, R., Hoey, T., Wathen, S. & Werritty, A. (1996) Field evidence for rapid downstream fining of river gravels through selective transport. *Geology*, 24(2), 179–182. Available from: [https://doi.org/10.1130/0091-7613\(1996\)024<0179:FEFRDF>2.3.CO;2](https://doi.org/10.1130/0091-7613(1996)024<0179:FEFRDF>2.3.CO;2)
- Ferguson, R.I., Sharma, B.P., Hodge, R.A., Hardy, R.J. & Warburton, J. (2017) Bed load tracer mobility in a mixed bedrock/alluvial channel. *Journal of Geophysical Research: Earth Surface*, 122(4), 807–822. Available from: <https://doi.org/10.1002/2016JF003946>
- Finnegan, N.J., Sklar, L.S. & Fuller, T.K. (2007) Interplay of sediment supply, river incision, and channel morphology revealed by the transient evolution of an experimental bedrock channel. *Journal of Geophysical Research*, 112(F3), F03S11. Available from: <https://doi.org/10.1029/2006JF000569>
- Goode, J.R. & Wohl, E. (2010) Substrate controls on the longitudinal profile of bedrock channels: Implications for reach-scale roughness. *Journal of Geophysical Research: Earth Surface*, 115(F3), F03018. Available from: <https://doi.org/10.1029/2008JF001188>
- Haschenburger, J.K. (2013) Tracing river gravels: Insights into dispersion from a long-term field experiment. *Geomorphology*, 200, 121–131. Available from: <https://doi.org/10.1016/j.geomorph.2013.03.033>
- Hassan, M.A., Saletti, M., Johnson, J.P.L., Ferrer-Boix, C., Venditti, J.G. & Church, M. (2020) Experimental insights into the threshold of motion in alluvial channels: Sediment supply and streambed state. *Journal of Geophysical Research: Earth Surface*, 125(12), e2020JF005736. Available from: <https://doi.org/10.1029/2020JF005736>
- Hodge, R.A. & Hoey, T.B. (2016) A Froude-scaled model of a bedrock-alluvial channel reach: 2. Sediment cover. *Journal of Geophysical Research: Earth Surface*, 121(9), 2015JF003709–1618. Available from: <https://doi.org/10.1002/2015JF003709>
- Hodge, R.A., Hoey, T.B. & Sklar, L.S. (2011) Bed load transport in bedrock rivers: The role of sediment cover in grain entrainment, translation, and deposition. *Journal of Geophysical Research: Earth Surface*, 116(F4), 1–19. Available from: <https://doi.org/10.1029/2011JF002032>
- Hodge, R.A., Voepel, H., Leyland, J., Sear, D.A. & Ahmed, S. (2020) X-ray computed tomography reveals that grain protrusion controls critical

- shear stress for entrainment of fluvial gravels. *Geology*, 48(2), 149–153. Available from: <https://doi.org/10.1130/G46883.1>
- Inoue, T., Izumi, N., Shimizu, Y. & Parker, G. (2014) Interaction among alluvial cover, bed roughness, and incision rate in purely bedrock and alluvial-bedrock channel. *Journal of Geophysical Research: Earth Surface*, 119(10), 2123–2146. Available from: <https://doi.org/10.1002/2014JF003133>
- Johnson, J.P.L. (2014) A surface roughness model for predicting alluvial cover and bed load transport rate in bedrock channels. *Journal of Geophysical Research: Earth Surface*, 119(10), 2147–2173. Available from: <https://doi.org/10.1002/2013JF003000>
- Johnson, J.P.L. (2016) Gravel threshold of motion: A state function of sediment transport disequilibrium? *Earth Surface Dynamics*, 4(3), 685–703. Available from: <https://doi.org/10.5194/esurf-4-685-2016>
- Kirchner, J.W., Dietrich, W.E., Iseya, F. & Ikeda, H. (1990) The variability of critical shear stress, friction angle, and grain protrusion in water-worked sediments. *Sedimentology*, 37(4), 647–672. Available from: <https://doi.org/10.1111/j.1365-3091.1990.tb00627.x>
- Lague, D. (2010) Reduction of long-term bedrock incision efficiency by short-term alluvial cover intermittency. *Journal of Geophysical Research-Earth Surface*, 115(F2), F02011. Available from: <https://doi.org/10.1029/2008JF001210>
- Lamarre, H. & Roy, A.G. (2008) A field experiment on the development of sedimentary structures in a gravel-bed river. *Earth Surface Processes and Landforms*, 33(7), 1064–1081. Available from: <https://doi.org/10.1002/esp.1602>
- Lamb, M.P., Dietrich, W.E. & Venditti, J.G. (2008) Is the critical shields stress for incipient sediment motion dependent on channel-bed slope? *Journal of Geophysical Research: Earth Surface*, 113(F2), 1–20. Available from: <https://doi.org/10.1029/2007JF000831>
- Lawless, M. & Robert, A. (2001) Three-dimensional flow structure around small-scale bedforms in a simulated gravel-bed environment. *Earth Surface Processes and Landforms*, 26(5), 507–522. Available from: <https://doi.org/10.1002/esp.195>
- Mao, L. (2012) The effect of hydrographs on bed load transport and bed sediment spatial arrangement. *Journal of Geophysical Research*, 117(F3), F03024. Available from: <https://doi.org/10.1029/2012JF002428>
- Masteller, C.C. & Finnegan, N.J. (2017) Interplay between grain protrusion and sediment entrainment in an experimental flume. *Journal of Geophysical Research: Earth Surface*, 122(1), 2016JF003943–2016JF003289. Available from: <https://doi.org/10.1002/2016JF003943>
- Miller, M.C., McCave, I.N. & Komar, P.D. (1977) Threshold of sediment motion under unidirectional currents. *Sedimentology*, 24(4), 507–527. Available from: <https://doi.org/10.1111/j.1365-3091.1977.tb00136.x>
- Mishra, J. & Inoue, T. (2020) Alluvial cover on bedrock channels: Applicability of existing models. *Earth Surface Dynamics*, 8(3), 695–716. Available from: <https://doi.org/10.5194/esurf-8-695-2020>
- Nelson, P.A. & Seminara, G. (2012) A theoretical framework for the morphodynamics of bedrock channels. *Geophysical Research Letters*, 39(6), L06408. Available from: <https://doi.org/10.1029/2011GL050806>
- Ockelford, A.-M. & Haynes, H. (2012) The impact of stress history on bed structure. *Earth Surface Processes and Landforms*, 38(7), 717–727. Available from: <https://doi.org/10.1002/esp.3348>
- Parker, G., Klingeman, P.C. & McLean, D.G. (1982) Bedload and size distribution in paved gravel-bed streams. *Journal of the Hydraulics Division-ASCE*, 108(4), 544–571. Available from: <https://doi.org/10.1061/JYCEAJ.0005854>
- Sanguinito, S. & Johnson, J. (2012) Quantifying gravel overlap and dislodgement forces on natural river bars: Implications for particle entrainment. *Earth Surface Processes and Landforms*, 37(1), 134–141. Available from: <https://doi.org/10.1002/esp.2237>
- Schmeeckle, M.W., Nelson, J.M. & Shreve, R.L. (2007) Forces on stationary particles in near-bed turbulent flows. *Journal of Geophysical Research: Earth Surface*, 112(F2), 1–21. Available from: <https://doi.org/10.1029/2006JF000536>
- Sklar, L.S. & Dietrich, W.E. (2004) A mechanistic model for river incision into bedrock by saltating bed load. *Water Resources Research*, 40(6), W06301. Available from: <https://doi.org/10.1029/2003WR002496>
- Turowski, J.M. (2021) Upscaling sediment-flux-dependent fluvial bedrock incision to long timescales. *Journal of Geophysical Research: Earth Surface*, 126(5), e2020JF005880. Available from: <https://doi.org/10.1029/2020JF005880>
- Vollmer, S. & Kleinhans, M.G. (2007) Predicting incipient motion, including the effect of turbulent pressure fluctuations in the bed. *Water Resources Research*, 43(5), 1–16. Available from: <https://doi.org/10.1029/2006WR004919>
- Whiting, P.J. & Dietrich, W.E. (1990) Boundary shear stress and roughness over Mobile alluvial beds. *Journal of Hydraulic Engineering*, 116(12), 1495–1511. Available from: [https://doi.org/10.1061/\(asce\)0733-9429\(1990\)116:12\(1495\)](https://doi.org/10.1061/(asce)0733-9429(1990)116:12(1495))
- Wiberg, P.L. & Smith, J.D. (1985) A theoretical model for saltating grains in water. *Journal of Geophysical Research*, 90(C4), 7341–7354. Available from: <https://doi.org/10.1029/JC090iC04p07341>
- Wilcock, P.R. & Crowe, J.C. (2003) Surface-based transport model for mixed-size sediment. *Journal of Hydraulic Engineering*, 129(2), 120–128. Available from: [https://doi.org/10.1061/\(ASCE\)0733-9429\(2003\)129:2\(120\)](https://doi.org/10.1061/(ASCE)0733-9429(2003)129:2(120))
- Wohl, E. (2015) Particle dynamics: The continuum of bedrock to alluvial river segments. *Geomorphology*, 241, 192–208. Available from: <https://doi.org/10.1016/j.geomorph.2015.04.014>
- Yager, E.M., Schmeeckle, M.W. & Badoux, A. (2018) Resistance is not futile: Grain resistance controls on observed critical shields stress variations. *Journal of Geophysical Research: Earth Surface*, 123(12), 3308–3322. Available from: <https://doi.org/10.1029/2018JF004817>

How to cite this article: Hodge, R.A. & Buechel, M.E.H. (2022)

The influence of bedrock river morphology and alluvial cover on gravel entrainment. Part 2: Modelling critical shear stress. *Earth Surface Processes and Landforms*, 47(14), 3348–3360. Available from: <https://doi.org/10.1002/esp.5462>